# Comparison of the Reactions $p+d\rightarrow H^3+\pi^+$, $p+d\rightarrow He^3+\pi^0$ as a Test of Charge Independence*

KENNETH C. BANDTEL,† WILSON J. FRANK,† AND BURTON J. MOYER
*Radiation Laboratory, University of California, Berkeley, California*

(Received January 21, 1957)

The pair of reactions $p+d\rightarrow H^3+\pi^+$ and $p+d\rightarrow He^3+\pi^0$ have been investigated experimentally to see if the predictions of the theory of charge independence are fulfilled. Because of the low cross section (a few microbarns) and large background (heavy particles emitted at $\sim 10°$ lab) the results do not provide as critical a test as might be hoped. We find that there is a 50% chance that the ratio of the reaction cross sections $(p+d\rightarrow\pi^++H^3)/(p+d\rightarrow\pi^0+He^3)$ is between 2.0 and 2.6. Charge independence predicts that the ratio should be exactly two. The experimental difficulties would be less at higher proton energies; this method would seem to provide a very stringent test of charge independence if the comparison could be made with sufficient accuracy.

## INTRODUCTION

A STUDY comparing the reactions

$$p+d\rightarrow t+\pi^+$$

and

$$p+d\rightarrow He^3+\pi^0$$

would provide information for a stringent test of the hypothesis of charge independence of nuclear forces.[1,2]

Other experimental investigations of this hypothesis have been concerned with the reaction pair, $p+p\rightarrow\pi^++d$ and $n+p\rightarrow\pi^0+d$. Hildebrand measured the angular distribution of the $n+p\rightarrow\pi^0+d$ reaction[3]; Durbin, Loar, and Steinberger measured $d+\pi^+\rightarrow p+p$ for the same center-of-mass (c.m.) energy.[4] Both results closely fit the same angular distribution (i.e., $0.2+\cos^2\theta$), in agreement with the predictions of charge independence. Schluter measured the $n+p\rightarrow\pi^0+d$ reaction for incident neutron energies near 400 Mev.[5] He found the total cross section by integration (at a given c.m. energy) and compared twice the value with various total cross-section measurements of the $p+p\rightarrow\pi^++d$ reaction that have been made in this energy range. Schulter's data are based on 102 deuterons; total cross section and energy dependence are in agreement with the $\pi^+$ experiment, within the accuracy of the data.

The experimental results in this paper were obtained during the spring and summer of 1954.[6] In mid-1955, the experiment was intensively pursued again with various improvements and changes in instrumentation. Unfortunately the early results were not improved upon, because of the inherent experimental difficulties stemming from measuring a very low cross section (about a microbarn) yielding reaction products coming out at less than 10° from the beam direction.

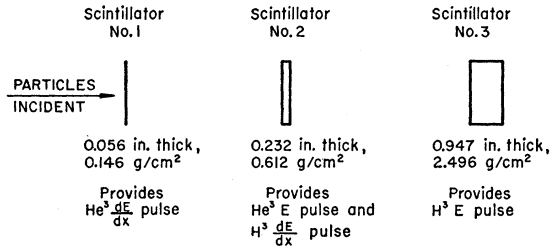


FIG. 1. Heavy-particle telescope—plastic scintillators. All scintillators are 4 in. square; the effective area is limited to a hole 3 in. in diameter by a lead collimator in front of the scintillators.

## II. EXPERIMENTAL DETAILS

### A. Method

A liquid deuterium target was bombarded by 340-Mev protons from the Berkeley 184-inch synchrocyclotron. The heavy particles, $H^3$ and $He^3$, are identified by measuring $dE/dx$ and $E$ at the selected

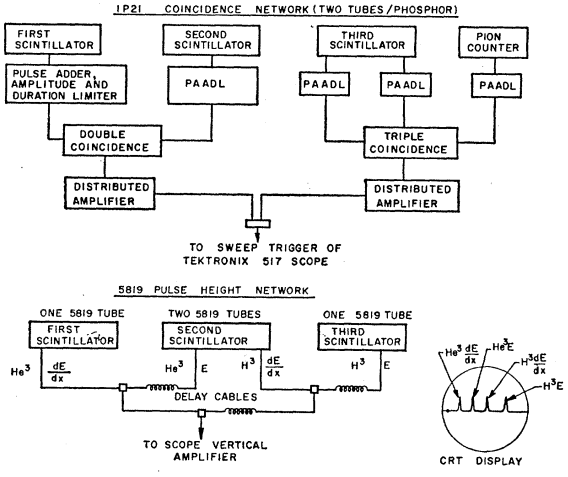


FIG. 2. Block diagram of electronics.

* This work was done under the auspices of the U. S. Atomic Energy Commission.

† Now at Radiation Laboratory, University of California, Livermore, California.

[1] A. M. L. Messiah, Phys. Rev. **86**, 430 (1952).
[2] M. Ruderman, Phys. Rev. **87**, 383 (1952).
[3] R. H. Hildebrand, Phys. Rev. **98**, 1090 (1953).
[4] Durbin, Loar, and Steinberger, Phys. Rev. **84**, 581 (1951).
[5] R. A. Schluter, Phys. Rev. **96**, 734 (1954).
[6] Bandtel, Frank, Madey, and Moyer, Phys. Rev. **95**, 639(A) (1954); Bandtel, Frank, Higgins, and Moyer, Phys. Rev. **98**, 269(A) (1955).

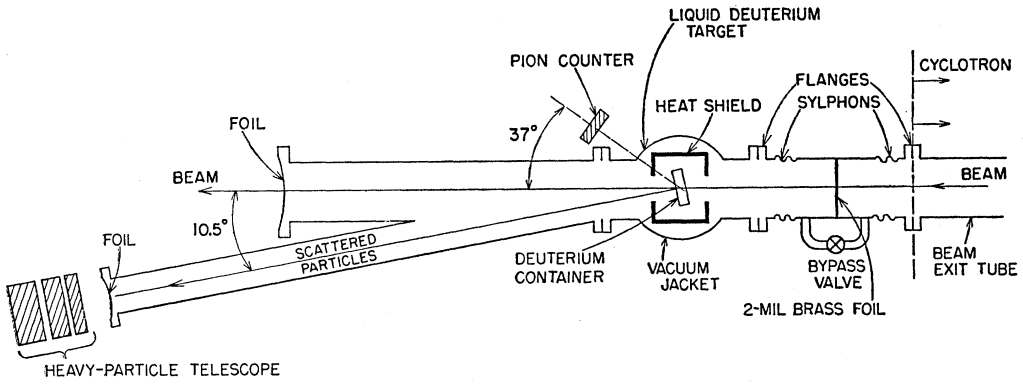


FIG. 3. Physical arrangement of the experiment (not to scale). Beam and scattered particles travel in evacuated tubes 4 in. in diameter.

angle. The $\pi^+$ is detected at its expected angle; the difference in time of flight[7] between it and the $H^3$ helps to identify the $p+d\rightarrow H^3+\pi^+$ process. The $\pi^0$ is not detected because of uncertainties in the efficiency of a gamma-ray counter, and because of the spreading of photons in the $\pi^0$ decay. The $p+d\rightarrow He^3+\pi^0$ process is identified only by the $He^3$ energy and ionization rate.

The two heavy particles are detected concurrently in a "heavy-particle telescope" consisting of three plastic scintillators (Fig. 1). The first scintillator is the $dE/dx$ counter for $He^3$; the second serves as both the $He^3$ $E$-counter and the $H^3$ $dE/dx$-counter; the third scintillator is the $H^3$ $E$-counter. For $He^3$ particles, a double coincidence is required between the first two scintillators. For $H^3$ particles a triple coincidence is required between the $\pi^+$ meson counter, delayed (owing to the $H^3$ time of flight), and the second and third scintillators of the telescope. The two types of events are measured concurrently, so that alternate runs to measure each process are not needed.

Each of the scintillators is viewed separately by 1P21 and 5819 photomultiplier tubes. The second scintillator is viewed by a double set of tubes for independent control of the $H^3$ and $He^3$ detection networks. The 5819 tubes provide pulse-height signals, and the 1P21 tubes provide signals for the coincidence circuit.[8] The coincidence circuit output triggers the sweep of a Tektronix 517 scope. The four 5819 tube signals are delayed, mixed, and fed to the scope vertical amplifier. Figure 2 shows the electronics block diagram. The traces are photographed by a continuously moving roll of 35-mm Linagraph Pan film. The pulse heights are read on a microfilm viewer, transcribed on records with the use of a dictaphone machine, and finally played back and plotted.

The pulse heights specify the coordinates of a point on a plot of $E$ *vs* $dE/dx$. Protons, deuterons, tritons, $He^3$ particles, etc., fall on separate lines on this plot, provided the resolution is sufficiently good. The position on the line depends on the energy of that particular kind of particle.

## B. Target

Figure 3 shows a schematic representation of the experimental arrangement. (The deuterium condenser was designed by Roscoe A. Byrns of this Laboratory.) The proton beam comes into the experimental area in an evacuated tube and passes through a 2-mil brass foil several feet upstream from the target. The foil prevents water or oil vapor from the cyclotron tank from condensing on the deuterium target, which is at liquid hydrogen temperature and would make an excellent trap for such volatile vapors. The beam continues to the target, which consists of a $\frac{3}{16}$-in. thick layer of liquid deuterium contained between two 1-mil

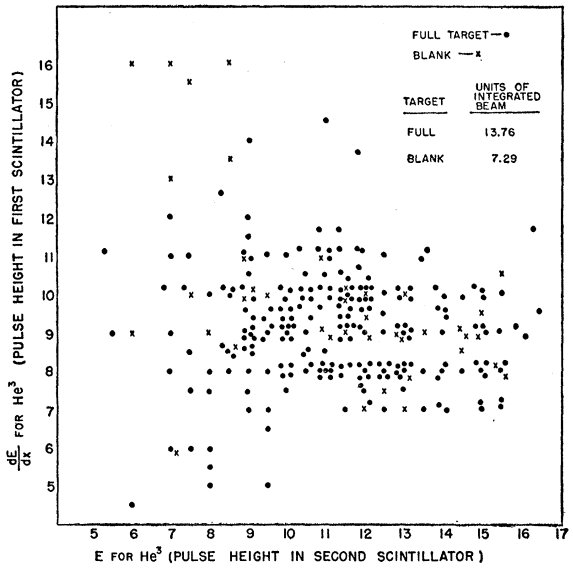


FIG. 4. $dE/dx$, $E$ plot for first and second scintillators. Particles that penetrate into the third scintillator have not been plotted because they have a range greater than that of the desired $He^3$ particles. (Protons, etc., occur below 7, 4 in great numbers; however, they pass through into the third scintillator and have not been plotted.)

[7] Frank, Bandtel, Madey, and Moyer, Phys. Rev. **94**, 1716 (1954).

[8] R. Madey, Rev. Sci. Instr. **26**, 971 (1955).

TABLE I.

| | Counts | Units of integrated beam | Counts per unit of integrated beam |
|---|---|---|---|
| Full target | 178 | 10.56 | ··· |
| Empty target | 36 | 6.29 | ··· |
| Difference (liquid deuterium events) | ··· | ··· | 11.2±1.6 |

stainless steel foils. A few feet after the target, the beam emerges through the exit foil into the atmosphere.

The vacuum jacket around the deuterium container (in which the deuterium is condensed by liquid hydrogen) is essential for providing heat insulation. The vacuum pipe for the scattered particles is necessary to prevent bad multiple scattering of the 85-Mev $He^3$ particles in air. Furthermore, it was found from a preliminary run that a 20-mil Dural window in the beam exit tube, the intervening air, and an entrance foil in the target enclosure all contributed appreciably to the background; therefore it was clearly desirable to provide the essentially complete vacuum path as shown. Since the thickness of the liquid deuterium plus the foils that contain the liquid deuterium is limited to about 0.09 g/cm² by multiple-scattering requirements for the $He^3$ particle, it can be seen that even the two 1-mil foils that contain the liquid deuterium (0.04 g/cm²) contribute appreciably to the background. The low differential cross section (only a few microbarns) intensifies this problem.

### C. Geometry and Kinematics

As shown on the experimental arrangement in Fig. 3, the heavy-particle telescope angle was 10.5°, and the correlated angle for the $\pi^+$ particle was 37°. Because of the $\pi^+-\pi^0$ mass difference, the kinematics for the two reactions transform differently from the laboratory to the center-of-mass system. For the triton, 10.5° in the laboratory system corresponds to 129.03° in the center-of-mass system; for the $He^3$, 10.5° lab corresponds to 134.35° c.m. Because of this effect, the experimentally measured ratio has to be corrected in accordance with the previously measured[7] angular distribution for the $p+d\rightarrow\pi^++H^3$ reaction so that the same c.m. angle is compared for both reactions.

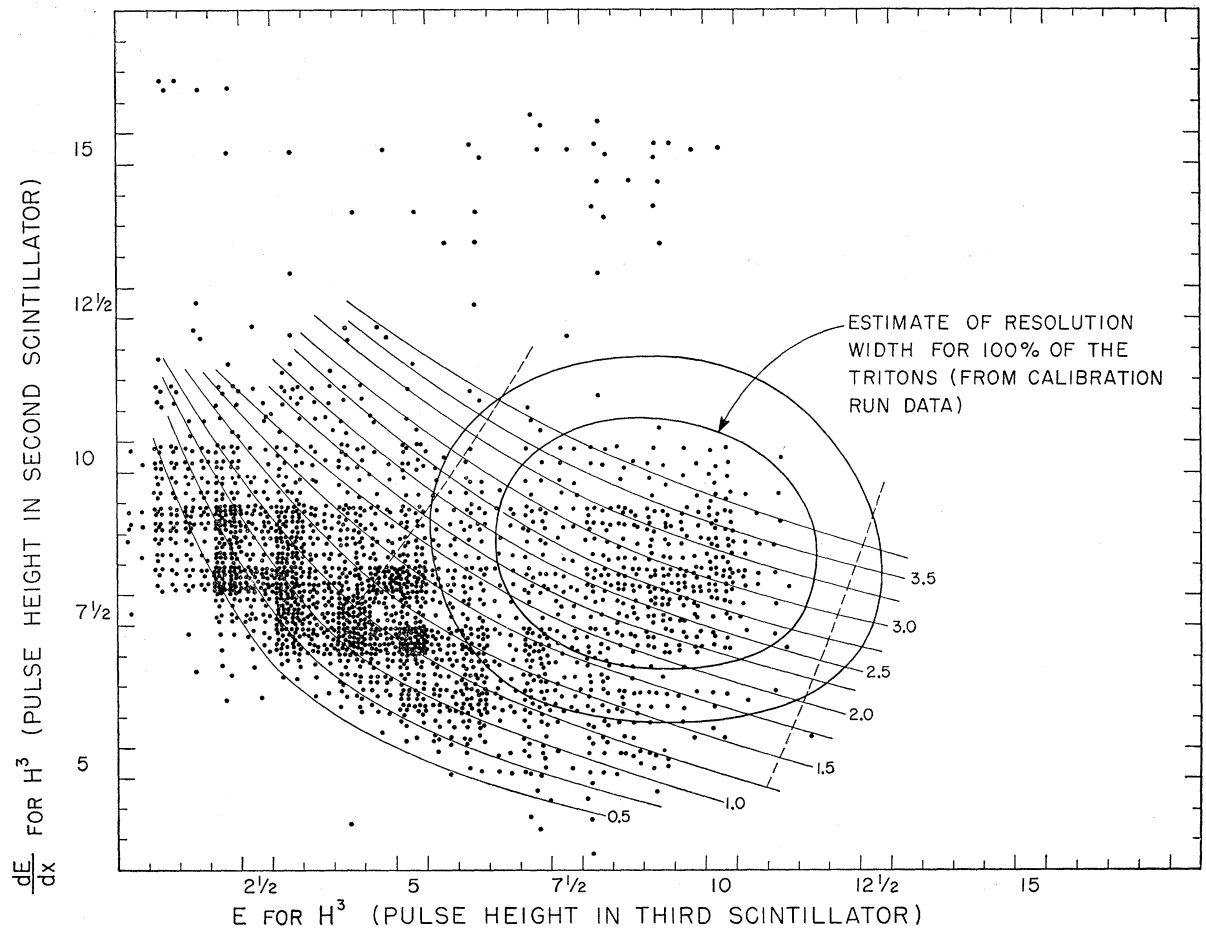


FIG. 5. $dE/dx$, $E$ plot for second and third scintillator liquid deuterium in target; 10.56 units of integrated beam.

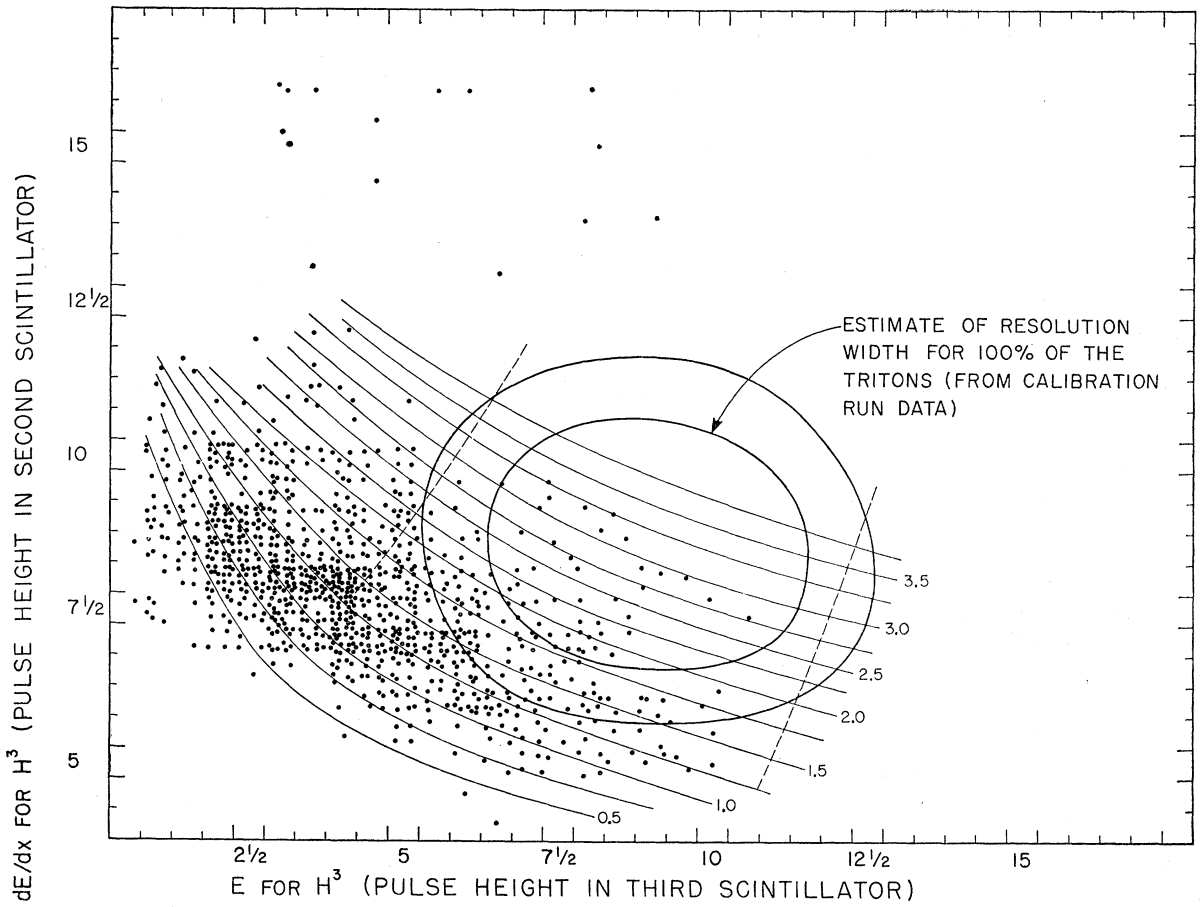


FIG. 6. *dE/dx*, *E* plot for second and third scintillators; empty target; 6.29 units of integrated beam.

## III. RESULTS OF THE EXPERIMENT

### A. Reduction of Data

#### *1. He³ Particles*

Figure 4 shows the results of plotting the pulse height in the first scintillator *vs* the pulse height in the second scintillator, considering only those particular cases in which the particle stopped in the second scintillator. The scintillator thicknesses have been arranged so that $He^3$ particles of the expected energy (85 Mev) should stop in the second scintillator. Many more pulses passed through into the third scintillator than stopped in the second. Many slow protons and other singly charged particles would appear in the lower left corner of the plot, but they all enter the third scintillator and so have not been plotted. The gains and voltages were set so that 85-Mev $He^3$ particles would appear at approximately (10,10). This was accomplished by a preliminary calibration on the $He^3$ beam of the 184-in. cyclotron, which was degraded in energy. The degrading absorber was placed in the emergent beam of $He^3$ particles just after they were deflected from their cyclotron orbit, and the steering-magnet current was lowered to direct the 85-Mev $He^3$ particles into the experimental area. Calibration data showed that most of the $He^3$ particles should fall within $\pm 25\%$ of the centroid of the distribution. This is approximately true for the pulse height in the first scintillator. The pulse height in the second scintillator spreads more than this, owing to the spread in energy in escaping from different parts of the target.

It seems extremely probable that the events in the center of the plot represent $He^3$ or $He^4$ particles.

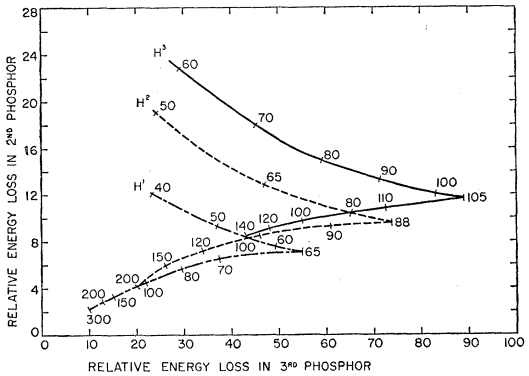


FIG. 7. Energy loss in second phosphor *vs* that in third phosphor.

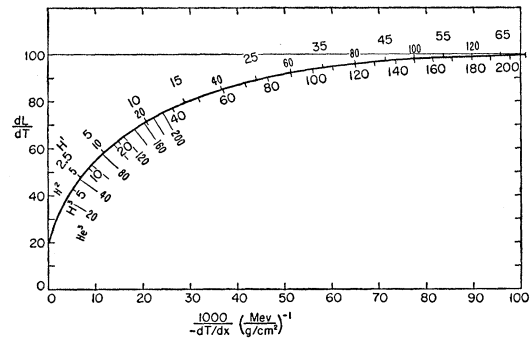


FIG. 8. Relative light output per unit energy loss in anthracene *vs* reciprocal specific energy loss. (The numbers arrayed along the curve refer to the kinetic energies of the indicated particles.)

However, $He^4$ particles could not be produced by bombarding deuterium by protons, and any $He^4$ particles produced from the foils are subtracted out in getting the difference counting rate. The final results are given in Table I.

Blank runs were accomplished by closing the exhaust valve above the target vessel, and slightly warming the latter electrically, so that the liquid phase was forced back out of the target into a reservoir by the pressure of deuterium vapor. It is estimated that the blank represents $\sim 2\%$ of the amount of deuterium contained when liquid deuterium filled the target (the presence of the foils contributes a background of about 30%).

### 2. $H^3$ Particles

Figures 5 and 6 show the results of plotting pulse heights No. 3 ($H^3$ $dE/dx$, Scintillator 2) and No. 4 ($H^3$ $E$, Scintillator 3) for the full- and empty-target runs. (Although Pulses 2 and 3 are both proportional to the light in the second scintillator, the $He^3$ $E$ pulse is almost an order of magnitude larger than the $H^3$ $dE/dx$ pulse. Since the dynamic range of the 517 scope vertical amplifier is just about an order of magnitude, two separate gain controls are necessary.) At first glance it is clear that a certain region of the full-target plot is more densely populated than in the empty-target plot; placing a line of demarcation, however, requires much consideration.

Figure 7 shows a plot of relative energy loss for protons, deuterons, and tritons in the second and third scintillators. Because of saturation effects when specific ionization is high (particle energy is low), an expected pulse-height plot would be considerably modified. The light produced per Mev of energy loss as a function of specific ionization is given in Fig. 8; this curve is derived from experimental data for a number of phosphors, but does not include our scintillator material—$(C_2H_2)_n$ plus a trace of terphenyl. It is assumed that saturation effects do not differ greatly from one *organic* scintillator to another.

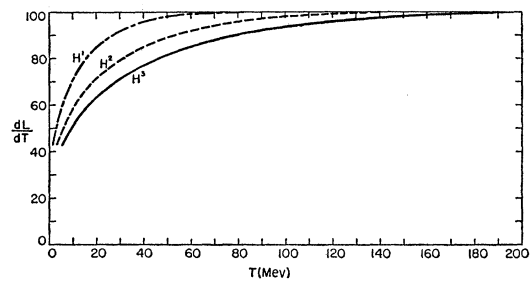


FIG. 9. Light output per unit energy loss *vs* kinetic energy.

Figure 8 may be transformed into the curves of Fig. 9 by use of the relation for $dT/dx$ *vs* $T$ for $(C_2H_2)_n$. From integration over appropriate intervals of $T$ under the curves of Fig. 9, we obtain the plots of relative light output in Fig. 10 corresponding to the relative energy losses shown in Fig. 7 for the phosphors employed. The curves of Fig. 10 would describe the distributions in Figs. 5 and 6 if resolution were perfect and light outputs were unique for similar events.

The $H^3$ pulse height counters were calibrated by using deuterons of such as energy as to give the same $dE/dx$ pulse as the expected tritons. The tritons were

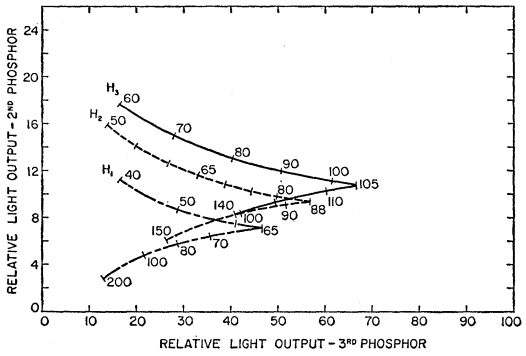


FIG. 10. Calculated light output from second phosphor *vs* that from third phosphor.

expected to fall around (10,10), but instead they appear centered about (8,9). By a trial and error process, the information from Fig. 10 has been fitted to the data in Figs. 5 and 6. The lines on Figs. 5 and 6 are lines of constant mass, representing the probable particle mass in multiples of the proton mass.

In Fig. 11, the number of particles per mass interval has been plotted against the mass; the trial and error procedure of calibrating the data involved centering the scattered proton peak around the proton mass location. Clearly, there are a number of mass-3 particles.

The triton peak can be seen more clearly by plotting the difference-counting ratio per unit interval of mass (Fig. 12). In determining the interval, the whole length of the lines of constant mass has been included. Since the tritons have an expected energy of $87 \pm 10$ Mev, the two dotted lines in Figs. 5 and 6 represent the expected limits. Figure 13 is a replot of Fig. 12 with the restricted triton data. Summed over these counts, the triton counting rate is $32.0 \pm 2.7$.

As another attempt to separate the tritons from the

background particles, two ovals have been drawn, centered on (8,9). The inner oval represents the 100% resolution width determined by the calibration run, while the outer oval is 50% larger, allowing for a margin of error. The resulting counting rates are 28.7±2.1 for the inner oval, and 31.5±2.9 for the outer one.

The counting rate seems relatively insensitive to the separation criteria; the first one (32.0±2.7 counts per unit of integrated beam) is used in subsequent calculations.

## B. Results

The $He^3$ and $H^3$ particles were measured at 10.5°. This means that the $\pi^0$ is at 45.65° c.m., and the $\pi^+$ is at 50.97° c.m. The measured angular distribution[7] of $p+d\rightarrow t+\pi^+$ was used to correct the $\pi^+$ to the same c.m. angle as the $\pi^0$, since we must compare the same angles in the center-of-mass system in order to test charge independence:

$$\frac{\dfrac{d\sigma}{d\Omega_{\text{c.m.}}}(\pi^+,45.7°)}{\dfrac{d\sigma}{d\Omega_{\text{c.m.}}}(\pi^0,45.7°)}=\frac{\dfrac{d\sigma}{d\Omega_{\text{c.m.}}}(\pi^+,51.0°)}{\dfrac{d\sigma}{d\Omega_{\text{c.m.}}}(\pi^0,45.7°)}\times\frac{\dfrac{d\sigma}{d\Omega_{\text{c.m.}}}(\pi^+,45.7°)}{\dfrac{d\sigma}{d\Omega_{\text{c.m.}}}(\pi^+,51.0°)},$$

and

$$\text{counting rate}\propto\frac{d\sigma}{d\Omega_{\text{c.m.}}}\frac{d\Omega_{\text{c.m.}}}{d\Omega_{\text{lab}}}\Delta\Omega_{\text{lab}},$$

$$\frac{d\sigma}{d\Omega_{\text{c.m.}}}\propto\frac{\text{counting rate}}{\Delta\Omega_{\text{lab}}}\left(\frac{d\Omega_{\text{lab}}}{d\Omega_{\text{c.m.}}}\right).$$

Therefore we have

$$\frac{\dfrac{d\sigma}{d\Omega}(\pi^+,45.7°)}{\dfrac{d\sigma}{d\Omega}(\pi^0,45.7°)}=\frac{\left(\begin{matrix}\text{counting rate}\\ \text{per unit beam}\end{matrix}\right)_{\pi^+}}{\left(\begin{matrix}\text{counting rate}\\ \text{per unit beam}\end{matrix}\right)_{\pi^0}}\times\frac{\dfrac{d\sigma}{d\Omega_{\text{c.m.}}}(\pi^+,45.7°)}{\dfrac{d\sigma}{d\Omega_{\text{c.m.}}}(\pi^+,51.0°)}\times\frac{\left(\dfrac{d\Omega_{\text{lab}}}{d\Omega_{\text{c.m.}}}\right)(\pi^+,51.0°)}{\left(\dfrac{d\Omega_{\text{lab}}}{d\Omega_{\text{c.m.}}}\right)(\pi^0,45.7°)}$$

$$\equiv\quad R_1\quad\times\quad R_2\quad\times\quad R_3.$$

$R_1$ is the raw data we get from the experiment. The error in this factor reflects the counting statistics of the experiment presented here.

$R_2$ is information we obtain from the previous experiment.[7] Unfortunately, we do not know this with much better accuracy than $R_1$. In order to get an estimate of $R_2$, we plotted the angular distribution data[7] and drew lines through the extremities of the probable errors. Then we read off values and probable errors at 45.7° and 51.0°, took the ratio, and compounded the error in the ratio, thus obtaining the value of $R_2$.

$R_3$ is just a matter of kinematical calculation. The following results were obtained:

$$R_1=\frac{32.0(\pm5.7\%)}{11.2(\pm9.6\%)}=2.86(\pm11.2\%);$$

$$R_2=\frac{2.90(\pm6.2\%)}{2.47(\pm4.1\%)}=1.175(\pm7.4\%);$$

$$R_3=(1/38.6)/(1/26.7)=0.692;$$

$$R_1R_2R_3=2.3(\pm13\%)=2.0\text{ to }2.6.$$

(Probable errors are quoted here.)

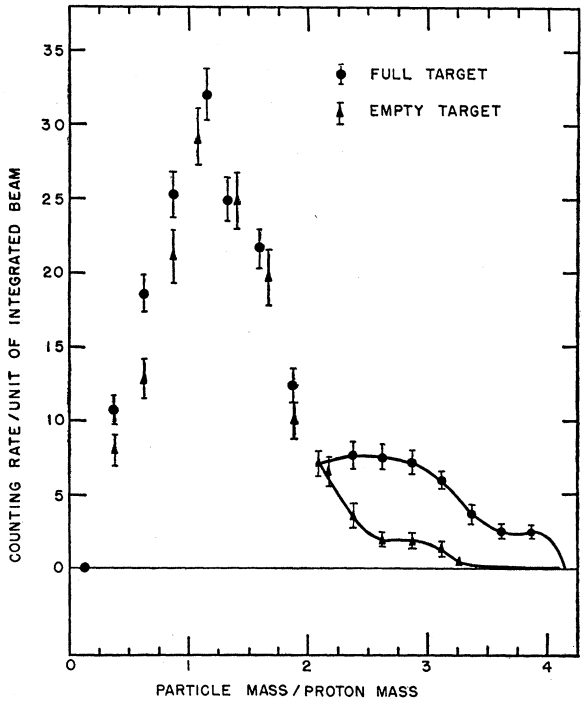


FIG. 11. Differential mass spectrum for second and third scintillators.

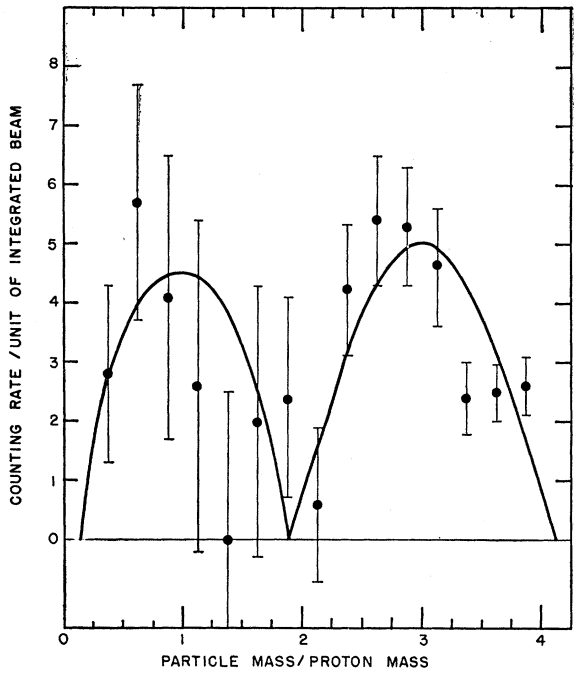


FIG. 12. Differential mass spectrum for second and third scintillators; [(full target)−(empty target)] per unit of integrated beam.

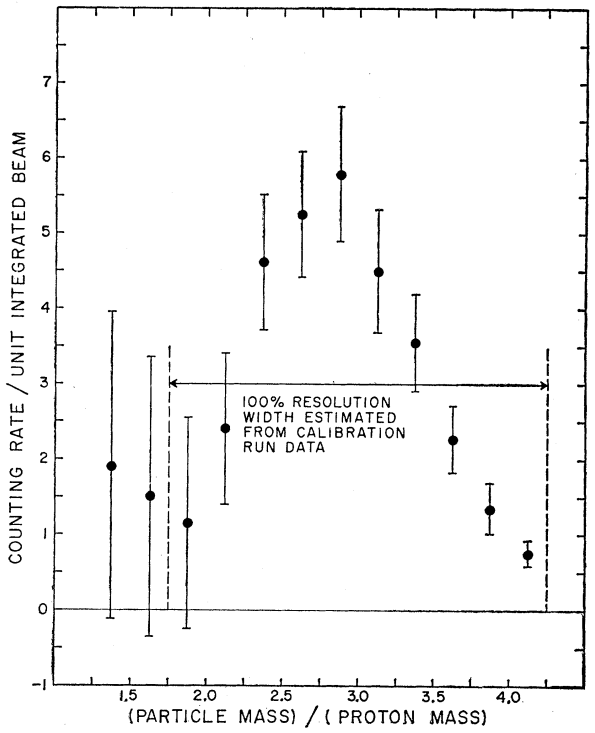


FIG. 13. Differential mass spectrum [(full target)−(empty target)] per unit integrated beam *vs* particle mass (in units of proton mass).

### C. Accuracy

A comparison experiment was done to minimize errors in beam monitoring, solid angle, etc. Nuclear interactions that result in the loss of the particle being detected are estimated to be negligible. In the thickest phosphor about 7% of the tritons suffer an inelastic nuclear interaction, and less than 7% are removed from the triton island, since an inelastic event does not always carry off energy in a way that does not produce light.

Consequently, it is believed that the biggest single contribution to the error is the counting statistics of this and the previous experiment.

### D. Interpretation

The results of this experiment indicate there is a 50% chance that the ratio of the reaction cross sections $(p+d\rightarrow\pi^{+}+\mathrm{H}^{3})/(p+d\rightarrow\pi^{0}+\mathrm{He}^{3})$ is between 2.0 and 2.6.

The statistical accuracy of the experiment is regrettably poor, but this is for the most part due to the low cross section of the reaction, which intensifies the detection and background difficulties.

One would have to say that the results of this experiment are in accord with the predictions of the hypothesis of conservation of isotopic spin, but in view of its poor statistical accuracy, this experiment does not provide a critical test of the conservation of isotopic spin.